Check for updates

A novel application of a multi-objective evolutionary algorithm in open channel flow modelling

S. Sharifi, M. Sterling and D. W. Knight

ABSTRACT

The Shiono and Knight method (SKM) is a simple depth-averaged flow model, based on the RANS equations which can be used to estimate the lateral distributions of depth-averaged velocity and boundary shear stress for flows in straight prismatic channels with the minimum of computational effort. However, in order to apply the SKM, detailed knowledge relating to the lateral variation of the friction factor (f), dimensionless eddy viscosity (λ) and a sink term representing the effects of secondary flow (Γ) are required. In this paper a multi-objective evolutionary algorithm is used to study the lateral variation and value of these parameters for simple trapezoidal channels over a wide range of aspect ratios through the model calibration process. Based on the available experimental data, four objectives are selected and the NSGA-II algorithm is applied to several datasets. The best answer for each set is then selected based on a proposed methodology. Rules relating f, λ and Γ to the wetted parameter ratio (P_b/P_w) for a variety of situations have been developed which provide practical guidance for the engineer on choosing the appropriate parameters in the SKM model.

Key words | evolutionary algorithms, modelling, NSGA-II, open channel flow, optimization

S. Sharifi (corresponding author)
M. Sterling
D. W. Knight
Department of Civil Engineering,
University of Birmingham,
Birmingham B15 2TT,
UK
Tel.: +44 121 414 5152
E-mail: *sxs650@bham.ac.uk*

NOTATION

B	semi width of trapezoidal channel bed
f	Darcy–Weisbach friction factor
F_i	non-dominated sorted fronts of R_t
$f_i(X)$	objective function
$F(X)$	vector of objectives
F_r	Froude number
g	gravitational acceleration
gen	number of maximum generations
H	water depth
k_s	roughness height
M	number of objective functions
N	number of variables
n	number of decision variables
pop	population size
P_b	wetted perimeter of the bed
P_c	crossover probability
P_m	mutation probability
P_t	parent population
P_w	wetted perimeter of the wall
Q	channel discharge
Q_t	offspring population
R	hydraulic radius
$\mathbb{R}$	set of real numbers
Re	Reynolds number
R_t	combination of parent and offspring population
s	side slope (1:s = vertical: horizontal)
S_o	channel bed slope
$\%SF_w$	percentage of shear force on the walls
u	streamwise velocity fluctuations
U	streamwise velocity
U_d	depth averaged streamwise velocity
U_*	shear velocity
v	transverse velocity fluctuations
V	transverse velocity
w	vertical velocity fluctuations
W	vertical velocity
x	streamwise coordinate

doi: 10.2166/hydro.2009.033

Downloaded from http://iwaponline.com/jh/article-pdf/11/1/31/386331/31.pdf
by guest

x_i decision variable
X variable vector
y lateral coordinate
z coordinate normal to bed
Γ transverse gradient of secondary flow term
$\bar{\varepsilon}_{yx}$ depth-averaged eddy viscosity
η_c real number GA crossover operator
η_m real number GA mutation operator
λ dimensionless eddy viscosity
ν kinematic viscosity
ρ fluid density
τ_b bed shear stress
$\bar{\tau}_{yx}$ depth-averaged Reynolds stress
Ω design domain search space
Ω_o objective domain search space

Subscripts

1–5 panel number
b bed
d depth
exp experimental data
i panel number
SKM predictions obtained using the SKM
t global value of either Q or $\%SF_w$
w wall

ACRONYMS

Asp Aspect ratio (2B/H)
EA Evolutionary Algorithms
EMO Evolutionary Multi-Objective
FCF Flood Channel Facility
GA Genetic Algorithms
NSGA-II Nondominated Sorting Genetic Algorithm II
RANS Reynolds-Averaged Navier–Stokes
SKM Shiono and Knight method
SBX Simulated Binary Crossover

INTRODUCTION

For many years, river modelling has been a core subject in the field of hydraulics. Over the past few decades, various attempts have been made to build models for flow in channels and rivers by understanding better the physical processes and simplifying the governing equations. Over these years river modelling has evolved from being predominately based on small-scale physical models in the laboratory into the present day emphasis on computational modelling of medium- to large-scale catchments.

The flow of water in channels is generally governed by the Reynolds-Averaged Navier–Stokes (RANS) Equations (Schlichting 1979) with the one-dimensional version of these equations known as the St. Venant Equations (Anderson 1997). The presence and formation of complex 3D structures, including various vortex structures along different planes, are significant constraints in precise modelling of flow in channels and rivers. As a consequence, the modelling of flow even in straight prismatic channels is surprisingly difficult (Nezu & Nakagawa 1993).

Simple depth-averaged RANS based models, such as the Shiono & Knight method (SKM), have been among the most popular methods used by researchers and have undergone significant developments in the last three decades (e.g. Vreugdenhil & Wijbenga 1982; Radojkovic & Djordjevic 1985; Wormleaton 1988; Samuels 1988, 1989; Shiono & Knight 1988, 1990, 1991; Lambert & Sellin 1996; Ervine *et al.* 2000; Spooner & Shiono 2003; Bousmar & Zech 2004). The SKM provides a tool for water level prediction (by estimating or extending stage-discharge curves), for distributing flows within a cross section (for damage assessments of buildings, eco-hydraulics and habitats) and for predicting the lateral distributions of boundary shear stress (for geomorphological and sediment transport studies). Its promising results, both for channels and rivers, have led it to being adopted by the UK's Environment Agency for use in its 'Conveyance and Afflux Estimation System' software (www.river-conveyance.net).

In order to apply the SKM successfully, in addition to the inputs of cross-sectional shape and longitudinal bed slope, detailed knowledge of the lateral variation of the friction factor (f), dimensionless eddy viscosity (λ) and a sink term representing the effects of secondary flow (Γ), are required. Initial guidance on choosing suitable values for f, λ and Γ for compound channels and simple rectangular channels has been provided by Knight and co-authors (Knight & Abril 1996; Abril & Knight 2004; Chlebek & Knight 2006). This paper extends this earlier

Downloaded from http://iwaponline.com/jh/article-pdf/11/1/31/386331/31.pdf
by guest

work significantly by providing detailed guidance relating to flow in homogeneous and heterogeneous prismatic trapezoidal channels over a wide variety of aspect ratios. Although the work presented in this paper deals with idealized channels, natural rivers are often schematized by such geometries in numerical models, and therefore it is envisaged that the results are generally applicable to natural rivers.

This paper is organized as follows: firstly, the SKM is described in detail and then the basics of multi-objective evolutionary algorithms are discussed. The experimental data used in the current work is briefly discussed followed by the calibration methodology and procedure. The results obtained from the application of the evolutionary algorithm are presented, enabling simple guidance rules to be developed. Finally, appropriate conclusions relating to the work are presented.

BACKGROUND

Shiono and Knight method of modelling

The SKM is a quasi-2D model that includes some of the key 3D flow structures that occur in rivers and compound channels. In this method, the depth-averaged momentum equation is solved for steady uniform turbulent flow in the streamwise direction (Shiono & Knight 1988, 1990, 1991).

The equation for the longitudinal streamwise component of momentum of a fluid element may be combined with the continuity equation to give

$$\rho\underbrace{\left[\frac{\partial UV}{\partial y}+\frac{\partial UW}{\partial z}\right]}_{\text{(I)}}=\underbrace{\rho g S_0}_{\text{(II)}}+\underbrace{\frac{\partial}{\partial y}(-\rho\overline{uv})}_{\text{(III)}}+\underbrace{\frac{\partial}{\partial z}(-\rho\overline{uw})}_{\text{(IV)}} \tag{1}$$

where ρ is the density of water, g the gravitational acceleration and S_0 the bed slope gradient. U, V and W are the mean velocity components and u, v and w are the velocity fluctuations in the x (streamwise), y (lateral) and z (vertical) directions, respectively. The overbar here indicates a time-averaged parameter. The physical meaning of the terms in Equation (1) are: (I) = secondary flow term, (II) = weight component term, (III) = vertical plane Reynolds stress term and (IV) = horizontal plane Reynolds stress term. Integrating (1) over the depth of water, the depth-averaged momentum equation becomes

$$\frac{\partial H(\rho UV)_d}{\partial y}=\rho g H S_0+\frac{\partial H\bar{\tau}_{yx}}{\partial y}-\tau_b\left(1+\frac{1}{s^2}\right)^{1/2} \tag{2}$$

where H is the water depth, τ_b the bed shear stress and s the side slope (1:s = vertical: horizontal). The depth-averaged terms are defined by

$$(\rho UV)_d=\frac{1}{H}\int_0^H(\rho UV)\mathrm{d}z \quad \text{and} \quad \bar{\tau}_{yx}=\frac{1}{H}\int_0^H(-\rho\overline{uv})\mathrm{d}z. \tag{3}$$

Using the Darcy–Weisbach friction factor and adopting the Boussinesq eddy viscosity model for the Reynolds shear stress, $\bar{\tau}_{yx}$, leads to the following expressions:

$$\begin{aligned} &f=\frac{8\tau_b}{\rho U_d}, U_*=\left(\frac{1}{8}f\right)^{1/2}U_d \quad \text{and} \\ &\bar{\tau}_{yx}=\rho\bar{\varepsilon}_{yx}\frac{\partial U_d}{\partial y}, \bar{\varepsilon}_{yx}=\lambda U_* H, \bar{\varepsilon}_{yx}=\lambda H\left(\frac{1}{8}f\right)^{1/2}U_d. \end{aligned} \tag{4}$$

Substituting Equations (3) and (4) into Equation (2) yields

$$\begin{aligned} &\rho g H S_o-\frac{1}{8}\rho f U_d^2\left(1+\frac{1}{s^2}\right)^{1/2}+\frac{\partial}{\partial y}\left\{\rho\lambda H^2\left(\frac{f}{8}\right)^{1/2}U_d\frac{\partial U_d}{\partial y}\right\} \\ &=\frac{\partial}{\partial y}[H(\rho UV)_d] \end{aligned} \tag{5}$$

where U_d is the depth averaged streamwise velocity, U_* the shear velocity, $\bar{\varepsilon}_{yx}$ the depth-averaged eddy viscosity, f the Darcy–Weisbach friction factor and λ the dimensionless eddy viscosity.

Based on experimental evidence, Shiono & Knight (1991) suggest that the depth-averaged secondary flow, $(\rho UV)_d$, may be approximated by constant values for a given element of the cross section. Using this concept, the lateral gradient of this term per unit length of the channel may then be written as

$$\frac{\partial}{\partial y}[H(\rho UV)_d]=\Gamma \tag{6}$$

This substitution enables Equation (5) to become a second-order linear differential equation and to be solved

Downloaded from http://iwaponline.com/jh/article-pdf/11/1/31/386331/31.pdf
by guest

analytically. The analytical solution to (5) may then be expressed for a constant depth, H, domain as

$$U_d = [A_1 e^{\gamma y} + A_2 e^{-\gamma y} + k]^{1/2} \tag{7}$$

where

$$k = \frac{8gS_0H}{f}(1-\beta);\ \gamma = \sqrt{\frac{2}{\lambda}}\left[\frac{f}{8}\right]^{1/4}\frac{1}{H} \quad \text{and} \quad \beta = \frac{\Gamma}{\rho g S_0 H}$$

and for a linear-side-slope domain as

$$U_d = \left[A_3\xi^{\alpha} + A_4\xi^{-\alpha-1} + \omega\xi + \eta\right]^{1/2} \tag{8}$$

where

$$\alpha = \frac{1}{2} + \frac{1}{2}\sqrt{1 + \frac{s(1+s^2)^{1/2}}{\lambda}(8f)^{1/2}};$$

$$\eta = \frac{\Gamma}{(1+s^2)^{1/2}\rho(f/8)};$$

$$\omega = \frac{gS_0}{(1+s^2)^{1/2}(f/8) - (\lambda/s^2)(f/8)^{1/2}}$$

and ξ is the depth function on the side-slope domain (e.g. $\xi = H - (y - B)/s$ for the main-channel side slope, where B = semi-width of main channel bed) and A_1 to A_4 are constants.

Once a cross section is divided into different panels, as shown in Figure 1, and the appropriate boundary conditions are applied, a set of linear equations can be obtained in which the A coefficients in Equations (7) and (8) are the unknowns. Solving these equations enables the lateral variation of depth–mean velocity across the channel to be obtained. Furthermore it is then possible to calculate the boundary shear stress distribution and the channel conveyance.

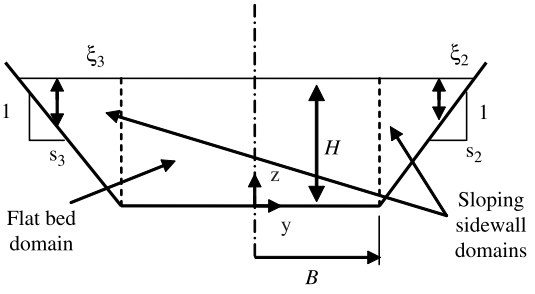

Figure 1 | Flat bed and sloping sidewall domains.

The accuracy of the SKM output directly depends on the selection of:

1. number, width and position of panels, and
2. lumped values for the friction factor, f, dimensionless eddy viscosity parameter, λ, and the secondary flow parameter, Γ, for each panel.

One of the main aims of this paper is to illustrate how a multi-objective evolutionary algorithm can be applied to physical experimental data for trapezoidal channels and how the lateral variation of three lumped parameters (f, λ and Γ) can be found through the process of model calibration. The final results provide guidance for practicing engineers in the selection of appropriate values for f, λ and Γ to implement within the SKM model.

Multi-objective optimization

Many practical problems involve multiple measures of performance, or objectives, which are competing or conflicting and need to be optimized simultaneously. Simple examples are maximizing profit and minimizing the cost of a product and maximizing performance and minimizing fuel consumption of a vehicle. The concept of optimizing multiple, but equally important, objectives was originally introduced by two economists, Edgeworth (in 1881) and Pareto (in 1897).

The general form of a multi-objective optimization problem can be defined as the minimization or maximization of a vector of objectives, $F(X)$, according to certain criteria:

$$\min \text{or} \max F(X) = \{f_1(X), f_2(X), \ldots, f_M(X)\} \tag{9}$$

$$\text{subject to}: g(X) \le 0 \quad \text{and} \quad h(X) = 0$$

where $X = (x_1, x_2, \ldots, x_N)$ is the decision variables vector in the domain search space, Ω, and $f_1(X), f_2(X), \ldots, f_M(X)$ are M objective functions that are to be minimized or maximized. Furthermore $g(X) \le 0$ and $h(X) = 0$ are inequality and equality constraints representing the majority of practical and physical constraints arising in engineering problems (Farina 2001). Accordingly, two subspaces known as the feasible design domain search space, Ω, and the objective

Downloaded from http://iwaponline.com/jh/article-pdf/11/1/31/386331/31.pdf
by guest

domain search space, Ω_0, are defined as

$$\Omega : \{X \in \mathbb{R}^N \, s.t. \, g(X) \leq 0 \quad \text{and} \quad h(X) = 0\} \tag{10}$$

$$\Omega_0 : \{F(X) \in \mathbb{R}^M \, s.t. \, X \in \Omega\} \tag{11}$$

where $\mathbb{R}$ is the set of real numbers and Ω_0 is the image of Ω through function F. It should be noted that, based on the nature of the problem, the design variables may not always belong to $\mathbb{R}^N$.

In contrast to single objective optimization problems, multi-objective optimization problems may not have a single solution which simultaneously satisfies all objectives to the same extent. In fact, there exists a set of equally good optimum solutions (trade-offs), none of which, without any further preference information, can be said to be better than the others.

Generally, when multiple solutions of a given multi-objective problem are available, in order to distinguish between better and worse solutions, it is necessary to rank them according to an order criterion. Based on the Pareto optima theory (Goldberg 1989), the solutions are ranked according to the Pareto dominance concept which is defined as:

For any two solutions X_1 and $X_2 \in \Omega$, and assuming a minimization problem, X_1dominates solution X_2 if:

$$f_i(X_1) \leq f_i(X_2) \quad \text{for all} \quad i \in [1, 2, \ldots, M] \tag{12}$$

$$f_j(X_1) < f_j(X_2) \quad \text{for at least one} \quad j \in [1, 2, \ldots, M]$$

In other words, if solution X_1 is not worse than X_2 in all objectives, but is strictly better in at least one objective, then it is said that X_1 dominates X_2.

Figure 2 illustrates a set of solutions for a typical two-objective problem where the goal is to minimize both objectives. The horizontal and vertical axes represent the value of the first and second objective, respectively, and each circle represents a decision vector (X_i) in the objective space (Ω_0). Based on the Pareto dominance concept, all empty circles are dominated by the filled ones. The union of all non-dominated solutions (filled circles) is called the Pareto set and its image in Ω_0 is known as the Pareto-optimal front. In fact, the Pareto front represents the best compromise solutions for which none has any precedence over any other. Once the Pareto front of a problem is found, the engineer is able to choose the best compromise solution according to the user's preferences.

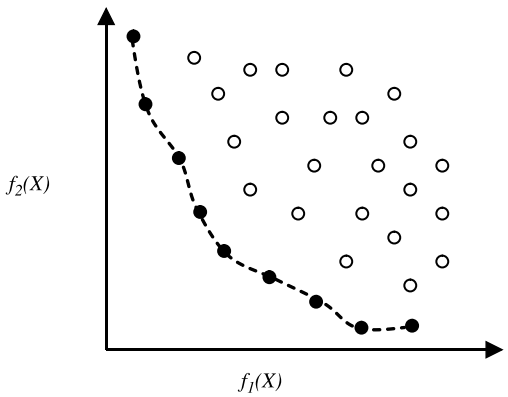

Figure 2 | The Pareto front of a two-objective optimization problem.

A variety of methods exist to solve multi-objective problems. The traditional methods convert multi-objective optimization problems into a series of equivalent single-objective problems and try to find the optimum solutions with conventional techniques (e.g. linear programming, gradient methods). The most frequently adopted methods and their limitations are listed below:

(1) In certain cases, objective functions may be optimized separately from each other and an insight gained concerning the 'best' that can be achieved in each performance dimension. Applying this method, suitable solutions to the overall problem can seldom be found. The optimal performance according to one objective, if such an optimum exists, often implies unacceptably low performance in one or more of the other objective dimensions (Fonseca & Fleming 1995).

(2) Aggregating approaches are methods which assign weights to each objective and then re-formulate a single objective by adding the weighted objectives and find the optimum of the new objective. These methods tend not to lead to a suitable solution as the decision regarding the 'best' solution relies to the so-called human decision-maker (Ghosh & Dehuri 2004).

(3) In the ε-constrained method (Hirschen & Schafer 2006) one of the objectives is selected as the main objective and the other objectives are imposed as constraints to the problem.

Downloaded from http://iwaponline.com/jh/article-pdf/11/1/31/386331/31.pdf
by guest

Although being relatively simple, at their best, these traditional techniques are only able to find one solution on the Pareto front at each run, i.e. for each equivalent single objective problem being solved, and hence are not convenient approaches towards solving a multi-objective problem.

Multi-objective evolutionary algorithms

Evolutionary Algorithms (EAs) are powerful global search methods that use mechanisms inspired by biological evolution, such as reproduction, mutation, recombination and selection, as their running engine. Because of their nature, EAs have the ability to handle complex problems, involving features such as discontinuities, multimodality and disjoint feasible spaces. In addition, they deal simultaneously with a set of possible solutions (population) which results in finding several members of the Pareto optimal set in a single run of the algorithm. These are the features that make them suitable for solving complex multi-objective problems (Fonseca & Fleming 1995).

The Non-dominated Sorting Genetic Algorithm II (NSGA-II) is a fast and elitist, second-generation evolutionary multi-objective (EMO) genetic algorithm proposed by Deb *et al.* (2002). The main features of this method are (Deb *et al.* 2002):

(1) At each generation, the best solutions found are preserved and included in the following generation using an elite-preserving operator.
(2) A fast algorithm is used to sort the non-dominated fronts.
(3) A two-level ranking method is used to assign the effective fitness of solutions during the selection process. At first, solutions are ranked according to their dominance rank and are organized in fronts of equal rank. Subsequently, within each front individual solutions are ranked according to a density measure using the crowding operator. Solutions residing in less crowded regions of the objective space are preferred.

Figure 3 illustrates the general procedure of this method. In this figure, P_t is the parent population, Q_t is the offspring population, R_t is the combined population ($R_t = P_t \cup Q_t$) and F_i are the non-dominated sorted fronts

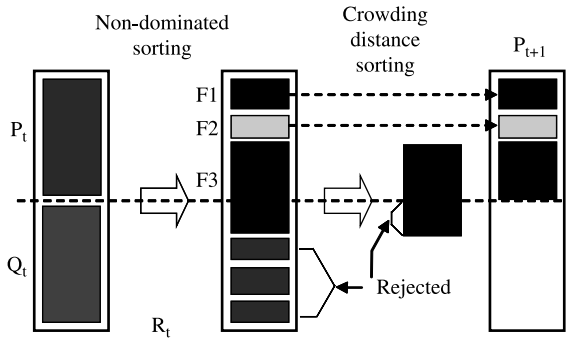

Figure 3 | Procedure of NSGA-II (Deb *et al.* 2002).

of R_t. For an in-depth explanation of this method the reader is referred to Deb *et al.* (2002).

Studying a variety of test cases (e.g. Deb *et al.* 2002; Khare *et al.* 2003), it has been shown that, compared to other elitist multi-objective evolutionary algorithms, NSGA-II has a better diversity preservation and therefore is able to compete with them regarding of its convergence to the true Pareto-optimal front in both constraint and non-constraint problems (Nazemi *et al.* 2006). This superiority has led to the successful application of NSGA-II in several real world problems such as long-term groundwater monitoring design (Reed *et al.* 2007), water distribution network design (Babayan *et al.* 2005), calibrating hydrological models (Liu *et al.* 2005; Bekele & Nicklow 2007), traffic signal timing optimization (Sun *et al.* 2003) and medicine (Lahanas *et al.* 2003).

Experimental data

Three sets of experimental data relating to uniform flow in trapezoidal channels were used in this paper: the Flood Channel Facility (FCF) Series 04 (Knight 1992), Yuen's (1989) data and Al-Hamid's (1991) data. This represented a combined total of 51 experimental test cases. The main motivation behind each dataset was to study the distribution of mean streamwise velocity and boundary shear stress for a wide range of simple trapezoidal channels with inbank flow under sub-and super-critical flow conditions.

The first dataset consists of detailed mean velocity and boundary shear stress distributions of 12 simple trapezoidal channels having a fixed bed width of 1.50 m, bed slope of 1.027×10^{-3}, side slope of 1:1 and varying depth, changing

Downloaded from http://iwaponline.com/jh/article-pdf/11/1/31/386331/31.pdf
by guest

between 0.296 m to 0.049 m to give aspect ratios (i.e. channel width/depth ratio = $2B/H$) between 5 and 30. For an in-depth analysis of this dataset the reader is referred to Knight & Sellin (1987) and Knight (1992). Yuen's (1989) data are based on uniform steady flow in trapezoidal channels with aspect ratios varying from 0.3 to 15. Detailed measurements of boundary shear stress distributions are available for all the channels, but the corresponding mean velocity distributions were only measured for 7 test cases. Five series of tests were undertaken at 5 different bed slopes (1.000, 3.969, 8.706, 14.52 and 23.37 ($\times 10^{-3}$)) and the side slopes were fixed at 1:1 through all the experiments. Al-Hamid's (1991) data were from experiments undertaken in simple trapezoidal open channels with both differentially and uniformly roughened boundaries for uniform, steady and fully developed turbulent flow. Two types of gravel distributions (d_{84} values of 18.0 and 9.3 mm, referred to as R1 and R2, respectively) were used for roughening the channel boundaries (i.e. walls only or walls and bed together). The experiments were conducted within the ranges of aspect ratio, $0.85 < 2B/H < 10.0$, Reynolds number, $3.4 \times 10^4 < \mathrm{Re} < 8.6 \times 10^5$, and Froude number, $0.39 < \mathrm{Fr} < 0.89$, for channel bed slopes 3.92×10^{-3}, 4.03×10^{-3} and 1.935×10^{-3} with 1:1 wall side slopes. Table 1 shows a summary of these three datasets and their test cases. Table 2 also shows a typical test case of the experimental data. In this table $\%SF_w$ is the percentage of shear force on the walls of the trapezoidal channel and y is the distance from the centreline of the channel. All these data, along with other data, are available on the website: www.flowdata.bham.ac.uk

Generally, once the normal depth conditions were established for a given discharge, individual velocity measurements were made within the cross section of each case using a small propeller meter and boundary shear stress measurements were made around the wetted perimeter of smooth beds using a Preston tube, together with the calibration equations of Patel (1965).

Over rough surfaces, local shear stresses were evaluated from point velocities measured close to the surface with a pitot-static tube. At the points where the local shear stresses were to be evaluated, three to five point velocities were measured at 5 mm spacings normal to the boundary surface. The local boundary shear stresses were then evaluated at 5 mm to 20 mm spacing intervals on the walls, using the corresponding logarithmic velocity law for turbulent rough flow, as indicated by Al-Hamid (1991).

The individual readings were subsequently numerically integrated and compared with the overall values, obtained respectively from a Venturi meter or the energy slope ($\tau_o = \rho g R S_o$). Typically, errors of $\pm 3\%$ and $\pm 6\%$ were tolerated in either integrated discharge or boundary shear.

CALIBRATION METHODOLOGY

The process of modifying the input parameters to a numerical model until the output from the model matches an observed set of data is best known as parameter estimation or model calibration. This procedure will result in finding the 'optimal' values of the immeasurable parameters in the model. In the following subsections, the methodology of investigating the lateral variation of three lumped parameters inside a channel through the process of calibrating a hydraulic model (e.g. SKM) via a multi-objective evolutionary algorithm (e.g. NSGA-II) is described.

Defining the panels

As mentioned before, one of the main issues in applying methods like SKM is defining the number, position and width of the panels within the cross section of the channel or river which is to be modelled. Continuing the work of Tominaga *et al.* (1989), Knight *et al.* (2007) proposed a panel structure for smooth trapezoidal channels based on the number and size of the observed contrarotating secondary flow cells and interpreting the secondary flow term (Γ). Figure 4 shows the required number of panels and their positon in order to apply the SKM.

Based on this analysis, the FCF experiments ($7.5 < 2B/H < 30$) were all modelled with five panels for half the channel and Yuen's data were modelled with four panels for cases with aspect ratios below 2.2.

In keeping with the above work on homogeneous channels, attention was now turned to the data of Al-Hamid (1991) in order to obtain the correct location of panels. Undertaking a thorough review of the experimental data for the two different cases, the panel structure illustrated in Figure 5 was selected.

Downloaded from http://iwaponline.com/jh/article-pdf/11/1/31/386331/31.pdf
by guest

Table 1 | Summary of all the datasets

Channel type	Test case	$2B$ (m)	H (m)		$2B/H$		P_b/P_w		S_0 ($\times 10^{-3}$)	Re ($\times 10^4$)		Fr		Q (l/s)	
			Min	Max	Min	Max	Min	Max		Min	Max	Min	Max	Min	Max
Smooth bed and smooth walls	FCF	1.500	0.049	0.301	4.980	30.850	0.352	2.181	1.027	6.317	99.151	0.584	0.762	29.900	656.300
	Yuen 000	0.150	0.050	0.150	1.000	3.000	0.354	1.061	1.027	4.101	15.638	0.559	0.590	3.500	26.300
	Yuen 200	0.150	0.029	0.099	1.515	5.263	0.536	1.861	8.706	7.145	35.804	1.882	2.000	4.700	41.100
	Yuen 400	0.150	0.029	0.099	1.515	5.263	0.536	1.861	23.370	12.443	61.831	3.243	3.227	8.100	66.300
Smooth bed and rough walls (R1)	Al-Hamid 01-05	0.107	0.043	0.126	0.850	2.491	0.601	1.761	3.920	3.489	11.870	0.520	0.544	2.009	13.688
	Al-Hamid 23-25	0.256	0.051	0.085	3.011	5.004	2.129	3.538	3.920	6.745	12.600	0.654	0.659	6.713	15.532
	Al-Hamid 26-30	0.399	0.040	0.067	5.989	9.987	4.235	7.062	3.920	7.130	13.302	0.853	0.884	9.300	20.053
Smooth bed and rough walls (R2)	Al-Hamid 09-13	0.121	0.048	0.142	0.849	2.513	0.601	1.777	3.920	4.257	14.730	0.607	0.638	3.113	21.947
	Al-Hamid 17-19	0.272	0.055	0.091	2.994	4.990	2.117	3.528	3.920	11.210	86.550	0.798	0.830	9.996	22.246
	Al-Hamid 31-35	0.416	0.042	0.070	5.986	10.005	4.233	7.074	1.935	5.623	11.610	0.690	0.708	8.030	18.470
Rough bed and rough walls (R1)	Al-Hamid 06-08	0.140	0.056	0.095	1.492	2.495	1.055	1.764	3.920	3.649	7.852	0.390	0.511	2.816	9.497
Rough bed and rough walls (R2)	Al-Hamid 14-16	0.143	0.057	0.095	1.505	2.516	1.064	1.779	3.920	3.714	7.852	0.440	0.511	3.313	9.497
	Al-Hamid 20-22	0.297	0.050	0.074	3.997	6.056	2.827	4.282	3.920	4.835	8.802	0.499	0.550	5.581	11.783
	Al-Hamid 36-38	0.441	0.044	0.059	7.491	9.982	5.297	7.058	4.030	4.453	7.029	0.493	0.540	6.660	11.430

Downloaded from http://iwaponline.com/jh/article-pdf/11/1/31/386331/31.pdf
by guest

Table 2 | A typical test case

Test case	Al-Hamid Exp 05	y (m)	U_d (m/s)	y (m)	τ (N/m^2)
$2B$ (m)	0.107	0.000	0.367	0.000	0.385
H (m)	0.0430	0.020	0.372	0.010	0.393
$2B/H$	2.49	0.040	0.346	0.020	0.407
P_b/P_w	1.76	0.070	0.212	0.030	0.384
S_0 ($\times 10^{-3}$)	3.920	0.080	0.159	0.040	0.308
Re ($\times 10^4$)	3.489	0.097	0.000	0.050	0.253
Fr	0.544			0.054	3.238
Q (l/s)	2.01			0.056	3.392
SF_w (%)	84.69			0.059	3.557
				0.064	3.085
				0.069	3.699
				0.073	2.021
				0.078	1.808
				0.083	0.898
				0.097	0.000

Optimization objective functions

Based on the available observed experimental data, four objective functions were identified (Equations (13)–(16)) to measure the difference between observed and model-generated data. As the mean streamwise velocity and local boundary shear stress distributions for each case consisted of many experimental points, the sum of squared errors (SSE) was selected as the goodness-of-fit measure. In contrast, the absolute percentage error (APE) was selected as the performance measure for the single measured and calculated values of discharge (Q) and the percentage of shear force on the walls of the channel (%SF_w):

$$f_1(X) = \sum_i ((U_d)_{SKM} - (U_d)_{exp})^2 \quad (13)$$

$$f_2(X) = \sum_i ((\tau_b)_{SKM} - (\tau_b)_{exp})^2 \quad (14)$$

$$f_3(X) = \left|\frac{Q_t - Q_{SKM}}{Q_t}\right| \times 100 \quad (15)$$

$$f_4(X) = \left|\frac{\%(SF_w)_t - \%(SF_w)_{SKM}}{\%(SF_w)_t}\right| \times 100 \quad (16)$$

where $X = (f_1,\lambda_1,\Gamma_1,\ldots,f_N,\lambda_N,\Gamma_N)$ is the variable vector in the design domain search space, Ω. The subscripts SKM and exp refer to the predictions obtained using the SKM model and experimental data, respectively. In $f_3(X)$ and $f_4(X)$ the subscript t is used to denote the global value of either Q or %SF_w and indicates that for these two functions the channel is considered as a whole, i.e. with the panels 'removed'. Depending on the available data, any combination of the above objectives can be minimized simultaneously. It is acknowledged that additional objective functions could have been used, e.g. one involving the friction factor. However, it is felt that those listed above made use of the best available data and enabled a good comparison with previously published experimental results.

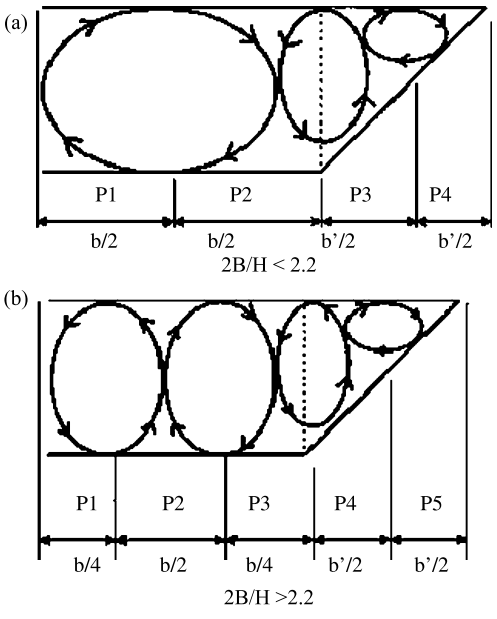

Figure 4 | Secondary flow cells and the number of panels for simple homogeneous smooth trapezoidal channels (Knight *et al.* 2007).

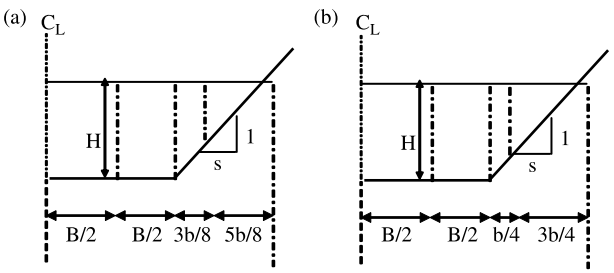

Figure 5 | Panel structure: (a) smooth bed and rough walls, (b) rough bed and rough walls.

Downloaded from http://iwaponline.com/jh/article-pdf/11/1/31/386331/31.pdf
by guest

Calibration procedure

In this paper, the calibration procedure was only performed on the test cases where the mean velocity and boundary shear stress distributions were available (i.e. all test cases of FCF and Al-Hamid's dataset and seven cases of Yuen's dataset). This restriction was imposed since past experience has shown that it is relatively easy to obtain either a reasonable prediction of depth-averaged mean velocity or boundary shear stress, but not both. In this two-stage procedure, the first two objectives (Equations (13) and (14)) were selected to be minimized simultaneously in the optimization stage and the latter two (Equations (15) and (16)) were used in the post-calibration validation process.

In the optimization stage, the real-coded NSGA-II algorithm with Simulated Binary Crossover (SBX) (Deb & Agarwal 1995) and polynomial mutation operators (Deb & Agarwal 1995) was used to calibrate the model on the trapezoidal channels with in-bank flow. A sensitivity analysis was first performed in order to obtain a robust algorithm parameter set (Table 3). The real-coded NSGA-II was run 30 times for each individual test case to limit the effect of randomness on the results. This resulted in a set of fronts of non-dominated solutions. Subsequently, the non-domination sort algorithm was applied on this set and an ultimate 'representative' Pareto front was found for each test case.

A post-validation process was then performed on the representative Pareto fronts with the aim of selecting an optimum variable set for each data case that has the following conditions:

(1) results in good smooth predictions of the mean streamwise velocity and local boundary shear stress distribution;

Table 3 | Real coded NSGA-II parameters used in this study

Operator	Value
Maximum number of generations (gen)	500
Population size (pop)	200
Crossover probability (P_c)	0.9
Crossover distribution index (η_c)	20
Mutation probability (P_m)	0.05
Mutation distribution index (η_m)	20

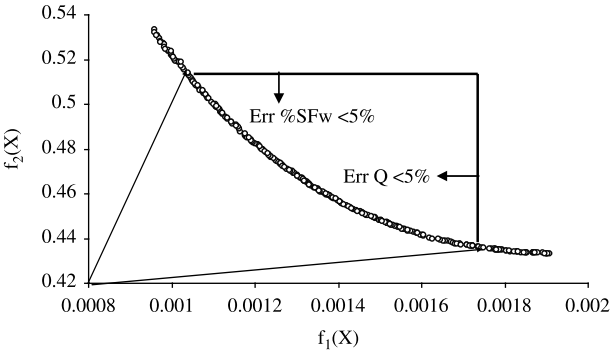

Figure 6 | Selecting the acceptable solutions on the Pareto front based on the value of the third and fourth objective function (case Al-Hamid Exp05).

(2) is able to predict the total discharge (Q) and percentage of shear force on the walls (%SF_w) with less than 5% error (Equations (15) and (16));

(3) inherits a proper Γ sign pattern in consecutive panels that is in accordance with the nature of the secondary flow cells which come in pairs (Perkins 1970; Knight *et al.* 2007).

The post-validation stage consisted of the following procedures:

- The third and fourth objective functions were evaluated for all the non-dominated solutions on the representative Pareto front. The effective portion of the Pareto front was found where all solutions resulted in estimating Q and %SF_w with less than 5% error (Figure 6).
- The solutions lying on the effective portion of the representative Pareto front were mapped to the decision search space (Ω). A non-hierarchical clustering analysis

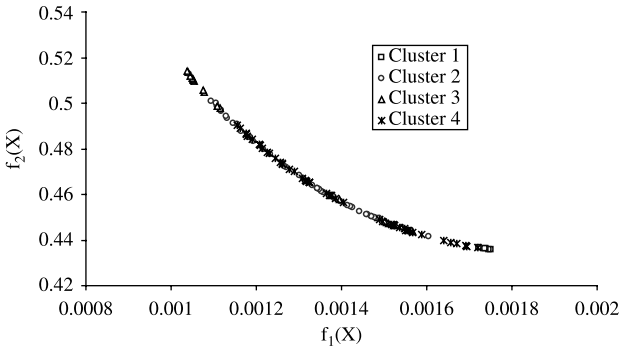

Figure 7 | The position of the found clusters on the front of the Pareto front (case Al-Hamid Exp05).

Downloaded from http://iwaponline.com/jh/article-pdf/11/1/31/386331/31.pdf
by guest

Table 4 | The most frequent observed patterns for the sign of the secondary flow term in different datasets

Sign of Γ		Panel 1	Panel 2	Panel 3	Panel 4	Panel 5
FCF data ($2B/H > 2.2$)	Pattern 1	−	+	+	−	+
	Pattern 2	−	+	−	−	+
Yuen's data ($2B/H < 3.0$)	Pattern 1	−	+	−	+	
	Pattern 2	+	+	−	+	
Al-Hamid's smooth bed and rough walls	Pattern 1	+	−	+	−	
	Pattern 2	−	+	+	−	
	Pattern 3	−	+	−	+	
Al-Hamid's rough bed and rough walls	Pattern 1	−	+	−	+	
	Pattern 2	−	+	+	−	
	Pattern 3	+	−	+	−	

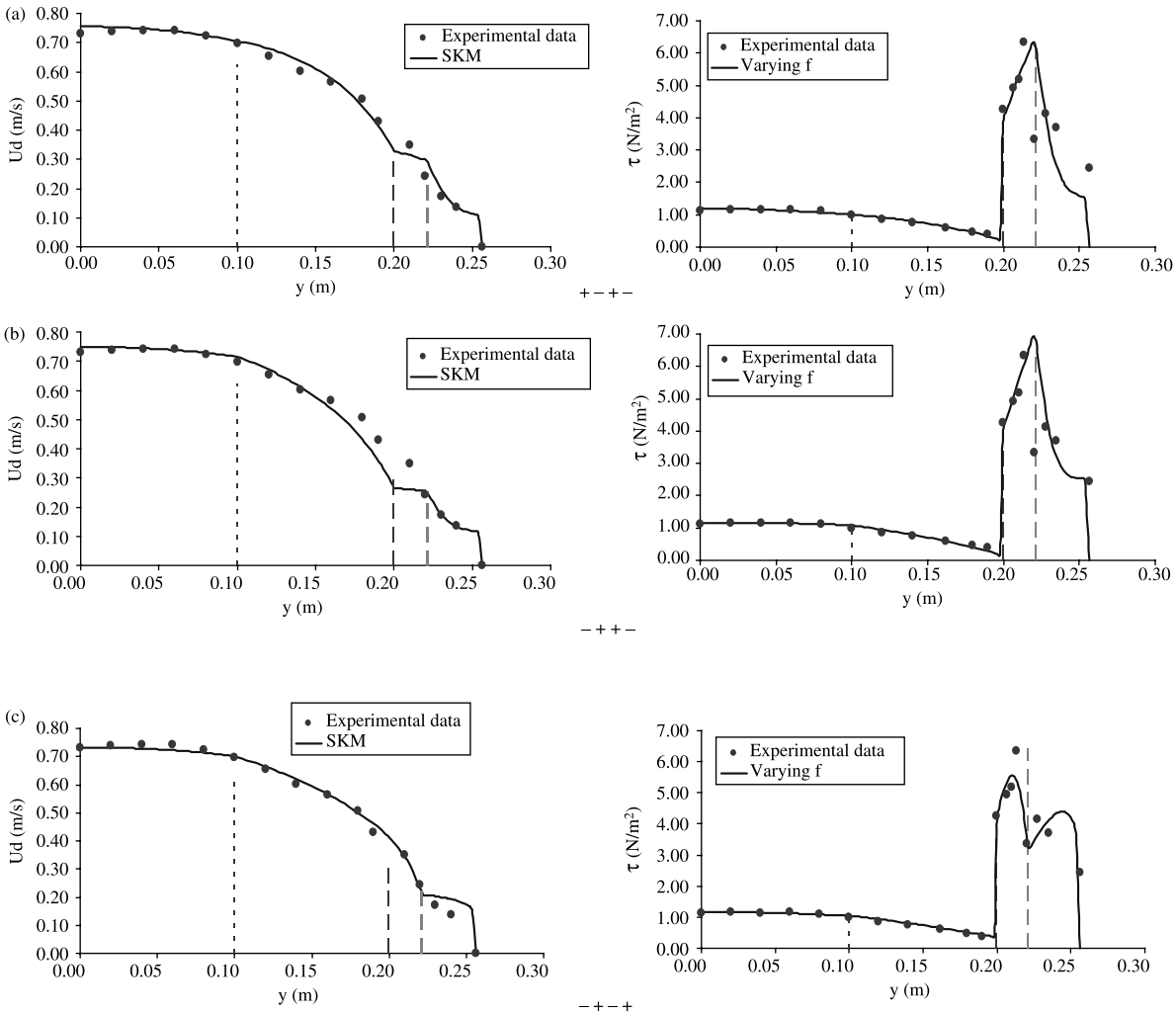

Figure 8 | Best mean velocity and boundary shear stress distribution of different patterns for Al-Hamid Exp27 (aspect ratio = 7.032, smooth bed and R1 on the wall). (The vertical dotted lines represent the panel intersections).

Downloaded from http://iwaponline.com/jh/article-pdf/11/1/31/386331/31.pdf
by guest

(k-means method) was then undertaken on the solutions and a number of clusters of solutions (between 3–7) were found for each test case. Figure 7 shows the position of the clusters on the Pareto front of a selected case.

- The major patterns for the sign of the secondary flow term (Γ) were recognized for each channel type (see Table 4) and the clusters which had the major patterns were preserved for each test case.
- The mode value of each variable in each of the remaining clusters was selected as the representative of that cluster and used in conjunction with the SKM to predict the depth-average streamwise velocity and boundary shear stress distributions. The obtained distributions were then plotted along with the experimental data for all cases. A typical set of results is illustrated in Figure 8.
- A cross-case analysis was then undertaken along with visual inspection on the obtained distributions of all cases in each data set. Based on the frequency of appearance of patterns in Pareto sets across cases and also the general look of the distributions, the dominant sign pattern of the secondary flow term (Γ) was selected for each dataset.
- For each test case, the predictions of the representatives (mode values) of clusters having the selected Γ sign pattern were compared and representatives resulting in similar distribution shapes were chosen as the best answer of each case.
- In a small number of cases, because of the non-uniqueness of the optimum parameter set, or as a result of overfitting the experimental data, the obtained optimum variable values were not in the same range as the other cases of the dataset. At this point, in order to be able to generalize the calibration results, the succeeding ranked non-dominated Pareto fronts were searched to find optimum solutions that not only had the selected Γ sign pattern, but also had optimum variables in the desired range.

RESULTS

Homogeneously roughened channels

Once the above procedure was completed for all of the homogeneously roughened cases, the best set of solutions (combination of f, λ and Γ for each panel) for each case were obtained and sorted based on the aspect ratio of the channel (e.g. see Table 5). Then the variation of each parameter was plotted against the wetted perimeter ratio (P_b/P_w) (Figure 9).

Table 5 | The optimal values of each parameter in different panels of Yuen's experiments

Test case		008	013	016	206	207	406	407
$2B/H$		2.00	1.50	1.00	2.05	1.52	2.05	1.52
P_b/P_w		0.71	0.53	0.35	0.73	0.54	0.73	0.54
Panel 1	f	0.0187	0.0170	0.0159	0.0150	0.0144	0.0144	0.0136
	λ	1.29	0.79	1.07	0.55	0.78	0.64	0.64
	Γ	−0.54	−0.57	−0.72	−0.79	−0.96	−0.97	−1.10
Panel 2	f	0.0207	0.0182	0.0171	0.0162	0.0157	0.0157	0.0149
	λ	0.38	0.28	0.16	0.11	0.11	0.12	0.12
	Γ	0.13	0.15	0.12	0.22	0.20	0.18	0.18
Panel 3	f	0.0221	0.0200	0.0185	0.0179	0.0167	0.0167	0.0159
	λ	0.84	0.82	0.71	0.29	0.24	0.22	0.20
	Γ	−0.36	−0.55	−0.64	−0.89	−1.14	−1.30	−1.41
Panel 4	f	0.0250	0.0228	0.0210	0.0194	0.0185	0.0185	0.0176
	λ	1.50	1.47	1.36	0.49	0.40	0.31	0.30
	Γ	0.79	0.89	0.96	1.70	1.80	1.91	1.98

Downloaded from http://iwaponline.com/jh/article-pdf/11/1/31/386331/31.pdf
by guest

The following conclusions can be drawn based from Figure 9 and the individual panel values of f_i, λ_i and Γ_i. The subscript i represents the panel number, starting from 1 for the panel adjacent to the centre line, and then increases progressively towards the edge of the channel.

(1) For trapezoidal channels with aspect ratios lower than 3.0 (Yuen's data), the friction factor increases almost linearly from the centreline of the channel towards the wall. For trapezoidal channels with aspect ratios between 7.5 and 30 (FCF data), the friction factor linearly increases from the first to the third panel, then appears to remain constant or reduce before increasing to its highest value in the fifth panel. This increase of f in shallower regions can also be explained by using the Colebrook–White equation, assuming a constant k_s for the channel.

(2) The value of the zonal friction factor in each panel is shown to increase with increase in the wetted perimeter ratio, P_b/P_w.

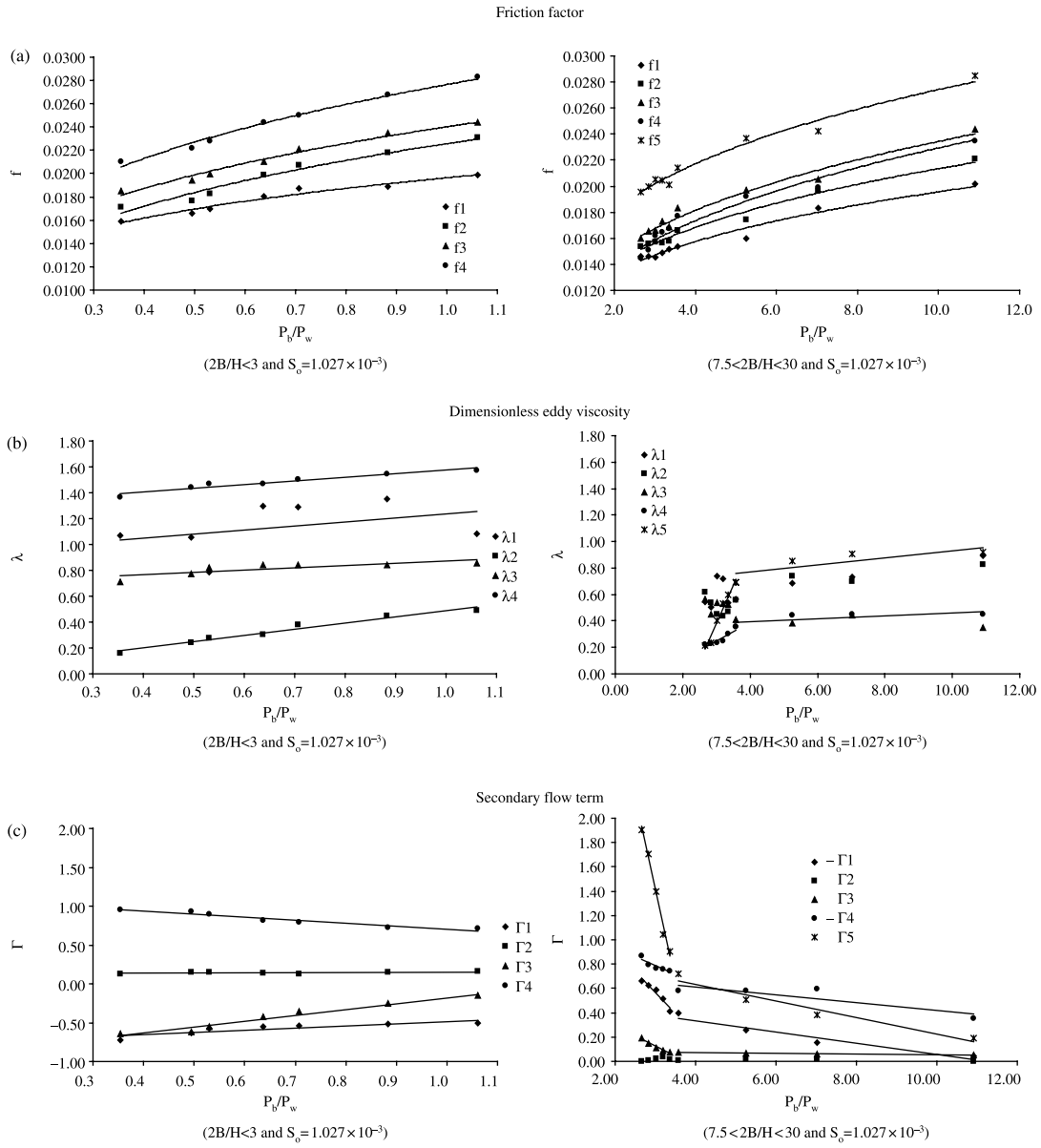

Figure 9 | f, λ and Γ vs. wetted perimeter ratio in channels with homogeneous roughness.

Downloaded from http://iwaponline.com/jh/article-pdf/11/1/31/386331/31.pdf
by guest

(3) The value of the dimensionless eddy viscosity does not appear to follow any specific pattern in the panels positioned in the constant depth region. This implies that the model is not sensitive to the value of this parameter in this region. In the panels on the sidewall region, the value of ε increases significantly as the wall is approached.

(4) For trapezoidal channels with aspect ratios higher than 7.5 (FCF data), the secondary flow term, Γ, is initially negative in the first panel and then rises towards zero in all cases. The value of this parameter then increases slightly in the third panel to a value near 0.10 before decreasing to a negative value in the fourth panel. Finally, a maximum positive value is obtained in the fifth panel. For trapezoidal channels with aspect ratios lower than 2.2 (Yuen's data), the variation of Γ is similar, except in the second panel where Γ is constant near 0.15. The high values of Γ for the panels in the sidewall region imply high levels of

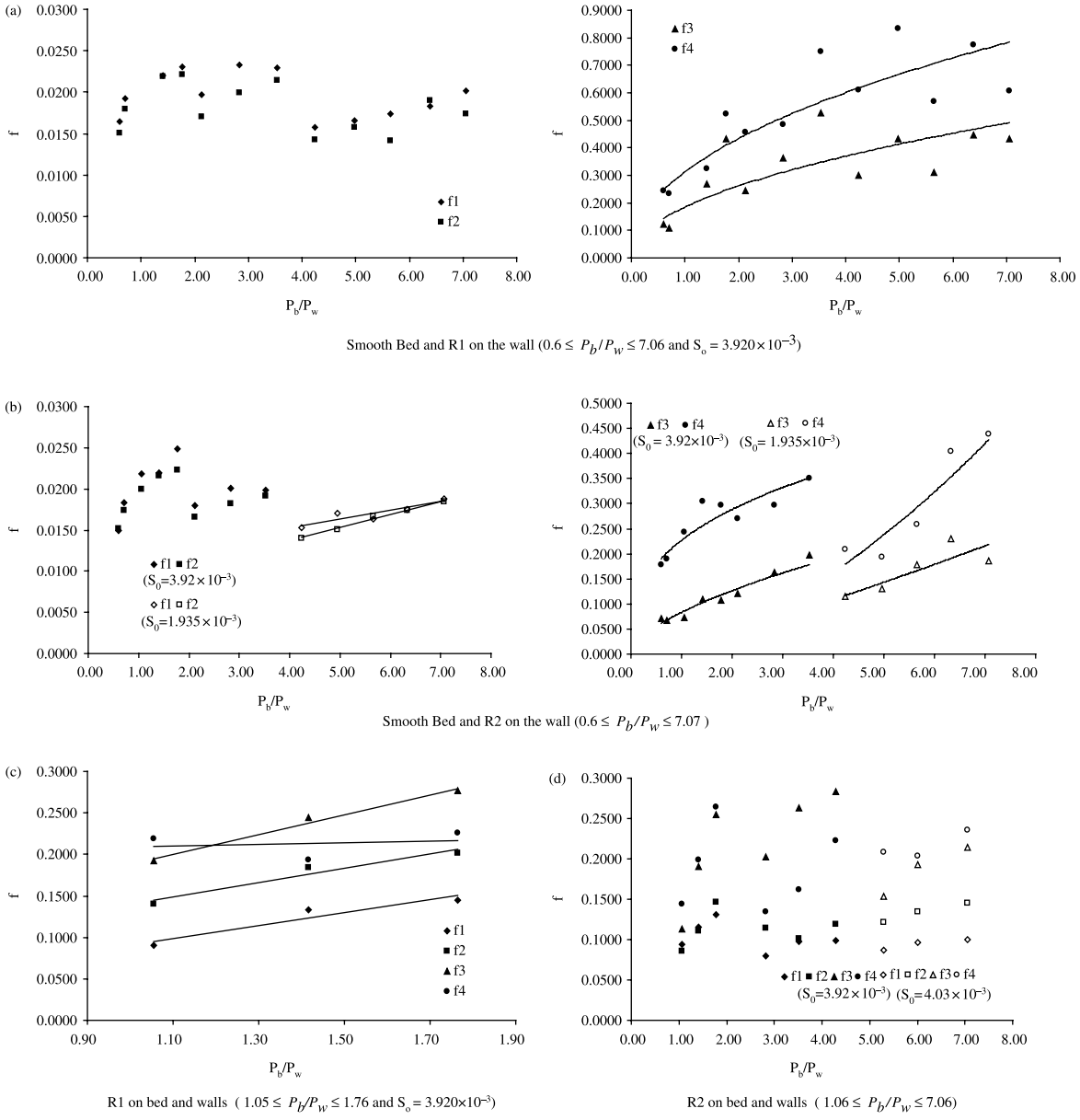

Figure 10 | Friction factor vs. wetted perimeter ratio in differentially and uniformly roughened trapezoidal channels.

Downloaded from http://iwaponline.com/jh/article-pdf/11/1/31/386331/31.pdf
by guest

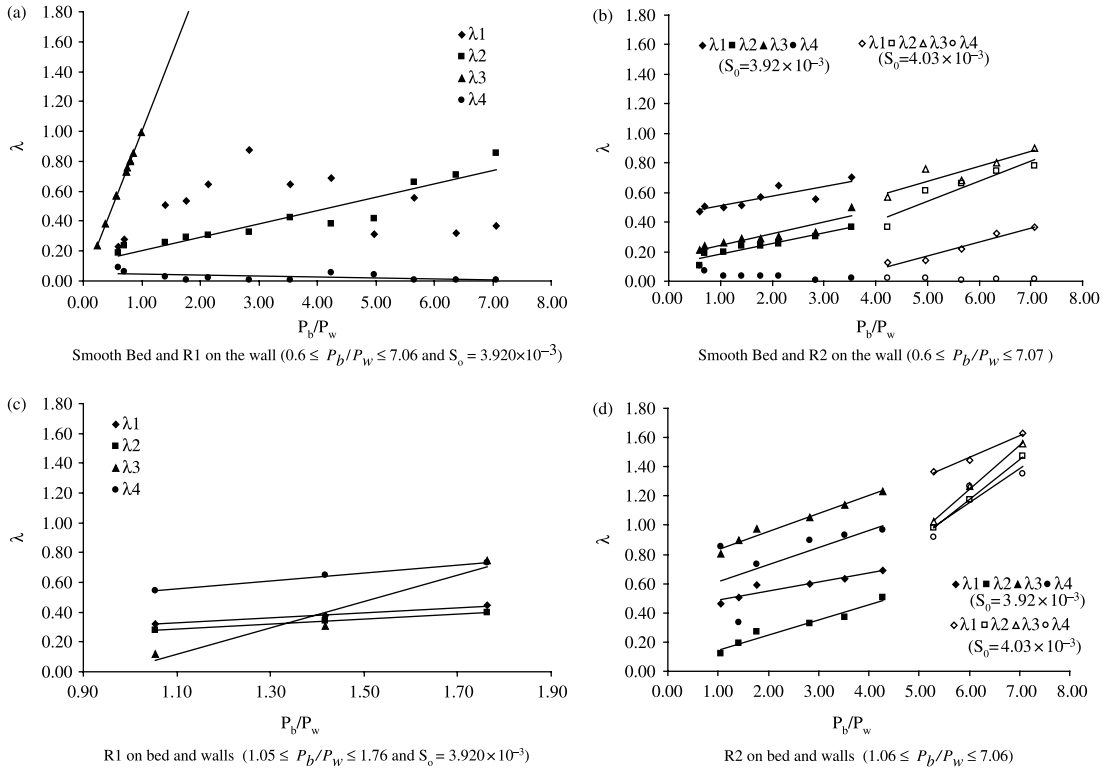

Figure 11 | Dimensionless eddy viscosity vs. wetted perimeter ratio in differentially and uniformly roughened trapezoidal channels.

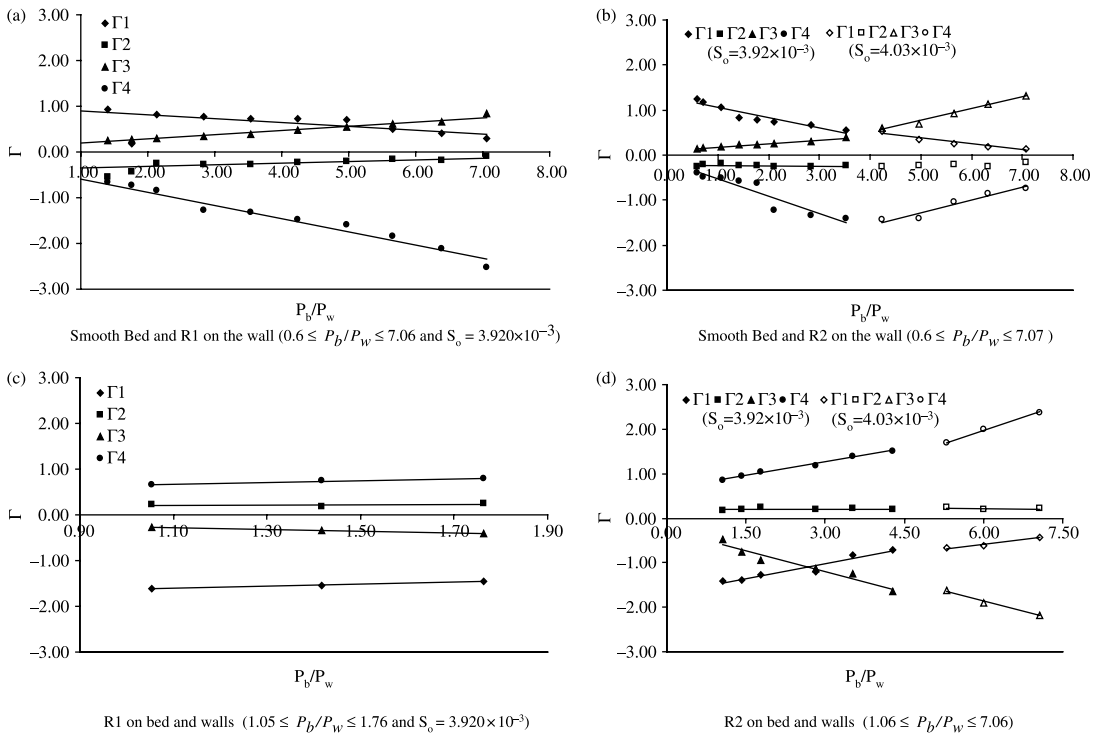

Figure 12 | Secondary flow term vs. wetted perimeter ratio in differentially and uniformly roughened trapezoidal channels.

Downloaded from http://iwaponline.com/jh/article-pdf/11/1/31/386331/31.pdf
by guest

circulation in these regions, which is consistent with the findings obtained from physical modelling. The pattern of negative and positive values found for Γ in adjacent panels also agrees with the findings of Knight *et al.* (2007).

(5) For different ranges of aspect ratios, the values of λ and Γ are linearly related to changes in wetted perimeter ratio.

Heterogeneously roughened channels

The same procedure was carried out for Al-Hamid's data and the best solution (set of f, λ and Γ in each panel) was obtained for each case. Figures 10–12 illustrate the results. The following conclusions can be drawn based on these figures and the individual panel values:

(1) For differentially roughened trapezoidal channels, Figures 10(a) and (b) show that the value of the friction factor in the second bed panel, f_2, is slightly lower than in the first panel, f_1. In the rough wall region the value of f increases significantly from the bed-wall intersection, f_3, to its maximum at the channel edge, f_4.

(2) Figures 10(a) and (b) also show that the values of the friction factors in the sloping sidewall region panels, f_3 and f_4, of differentially roughened channels increase with the increase in the wetted perimeter ratio.

(3) Figure 10(c) indicates that, for uniformly roughened channels with R1 on the bed and walls and a bed slope of 3.92×10^{-3}, the friction factor in all panels increases almost linearly with the increase in the wetted perimeter ratio, with an exception in the last panel where the friction factor remains more or less constant. Figure 10(d) also shows a somewhat similar pattern for channels with R2 on the bed and walls and a bed slope of 4.03×10^{-3}. In contrast, when the bed slope is reduced to 3.92×10^{-3} a general

Table 6 | Equations for finding the friction factor in each panel in the form of $f = a\,(P_b/P_w)^b$

Aspect ratio (2B/H)	Panel	a	b
0 < Asp < 3	1	0.0196	0.2122
	2	0.0226	0.2976
	3	0.0240	0.2719
	4	0.0277	0.2846
7.5 < Asp < 30	1	0.0113	0.2369
	2	0.0117	0.2594
	3	0.0123	0.2799
	4	0.0114	0.3049
	5	0.0153	0.2545

Table 7 | Equations for finding the dimensionless eddy viscosity in each panel in the form of $\lambda = a\,(P_b/P_w) + b$

Aspect ratio (2B/H)	Panel	a	b
0 < Asp < 3	1	0	0.60
	2	0.4832	0.0054
	3	0.1773	0.6933
	4	0.2773	1.2965
7.5 < Asp < 10	1	0	0.60
	2	0	0.60
	3	0	0.60
	4	0.1442	−0.1822
	5	0.5754	−1.3427
10 < Asp < 30	1	0	0.60
	2	0	0.60
	3	0	0.60
	4	0.0107	0.3513
	5	0.0274	0.6583

Table 8 | Equations for finding the secondary flow term in each panel in the form of $\Gamma = a\,(P_b/P_w) + b$

Aspect ratio (2B/H)	Panel	a	b
0 < Asp < 3	1	0.2739	−0.7593
	2	0	0.15
	3	0.7548	−0.9331
	4	−0.3911	1.0928
7.5 < Asp < 10	1	0.3459	−1.6026
	2	0	0.01
	3	−0.1712	0.6371
	4	0.1581	−1.2626
	5	−1.5306	6.0043
10 < Asp < 30	1	0.0465	−0.5221
	2	0	0.01
	3	−0.0024	0.0785
	4	0.0320	−0.7419
	5	−0.0689	0.9101

Downloaded from http://iwaponline.com/jh/article-pdf/11/1/31/386331/31.pdf
by guest

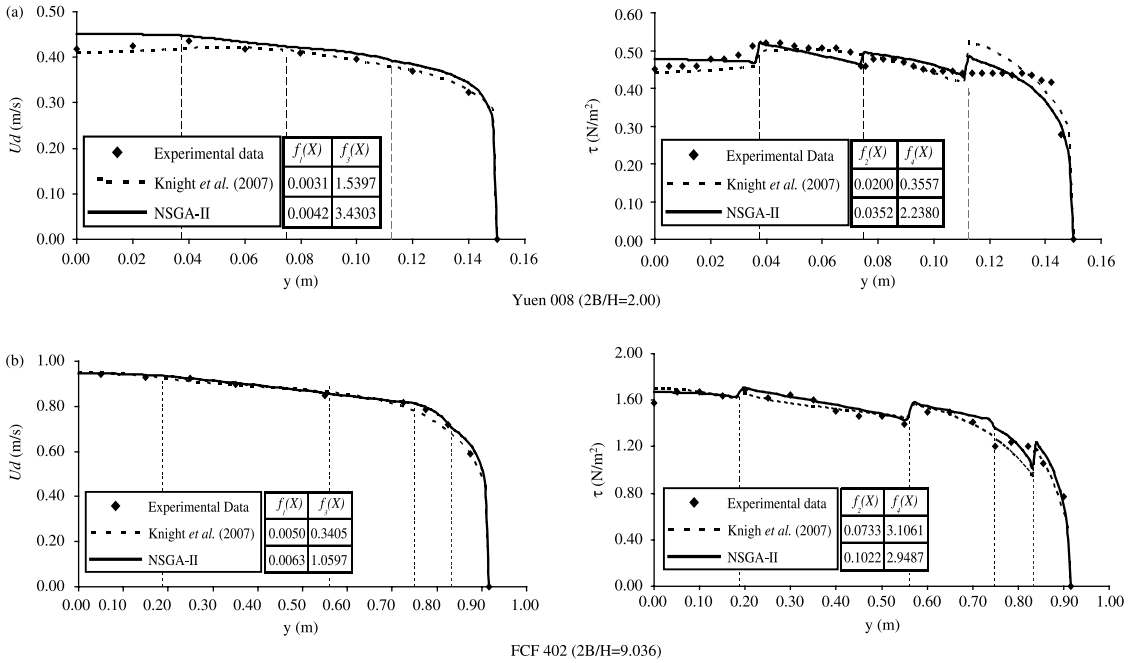

Figure 13 | Comparing the predictions of the calibrated SKM with two examples taken from Knight *et al.* (2007) (the vertical dotted lines represent the panel intersections).

trend for the lateral variation of the friction factor cannot be recognized.

(4) The optimum values found for λ in the smooth bed region of partially roughened channels are again scattered. This again implies that the model is not sensitive to λ in these smooth regions. On the other hand, the model is very sensitive to the value of λ in the third and fourth panels.

(5) Figures 11(c) and (d) indicate that, in homogeneously roughened channels, the zonal dimensionless eddy viscosity, λ, increases with the increase in the wetted perimeter ratio, P_b/P_w.

(6) The best pattern for the sign of Γ in differentially roughened channels is found to be $+ - + -$, which is exactly the opposite pattern found for uniformly smooth and uniformly roughened channels. This change in the sign of Γ can be interpreted as a change in the rotating direction of all the secondary flow cells.

(7) The lateral variation of the absolute optimum values of Γ is similar to that of homogeneously roughened channels. The absolute value of Γ in the second panel of all cases again converges to a value near 0.25, which is slightly different from the smooth cases. The important difference is that the maximum value of Γ for differentially roughened channels does not appear in the final panel.

Preliminary parameter guidelines

The results of calibrating the model according to various datasets reveal how each of these parameters changes with respect to aspect ratio and panel number. Furthermore, in order to add to the degree of applicability of the results, an attempt has been made to provide guidance on choosing the appropriate values of f, λ and Γ in smooth homogeneous trapezoidal channels. Based on this initial exploratory work, a set of equations has been proposed which relate the values of f, λ and Γ in each panel to the channel's wetted perimeter ratio (Tables 6–8). It should be noted that, for panels in which the model is not sensitive to the value of the zonal dimensionless eddy viscosity, a constant value of 0.6 is selected for this parameter. These preliminary guidelines provide some practical rules for the engineer in choosing the appropriate parameters for use in the SKM model. It is the intent that these preliminary parameter guidelines be updated shortly in the light of other objective functions that

Downloaded from http://iwaponline.com/jh/article-pdf/11/1/31/386331/31.pdf
by guest

are more physically based and take into account likely parameter values from all available experimental sources.

In order to demonstrate the advantages of the proposed approach over previous calibration attempts, a comparison was made with two examples taken from Knight *et al.* (2007). Figure 13 shows the depth-averaged velocity and boundary shear stress distributions for two smooth homogeneous test cases along with the calculated values of the four objective functions (Equations (13)–(16)). It is observed that the predictions of the SKM calibrated with the NSGA-II algorithm not only gives slightly better results in terms of both the general shape of the distributions and values of the objective functions, but is also an automated process and does not rely on 'fitting by eye'. It can thus be applied to many datasets with ease.

CONCLUSIONS

(1) Previous research (e.g. Knight & Shiono 1996; Abril & Knight 2004; McGahey *et al.* 2006) has demonstrated that the SKM is capable of modelling channels and rivers of various cross sections both accurately and with a minimum of computational effort, provided certain guidelines are followed. One of the major issues concerning the application of the model relates to the most appropriate values of f, λ and Γ for each panel within the channel. Through the application of a multi-objective evolutionary algorithm, this paper has attempted to provide guidance for choosing three parameters values required for modelling flow in smooth homogeneous trapezoidal channels.

(2) It has been shown that the multi-objective evolutionary algorithm implemented (NSGA-II) is a powerful tool for detailed critical analysis of lumped parameters within a RANS-based model, in supporting a considerably difficult model calibration problem. Furthermore, the parameter guidance equations can be easily used by engineers to model inbank flow in smooth homogeneous trapezoidal channels. This is of particular practical significance since these are among the most common cross sections encountered in many open channel flow problems, including rivers and irrigation channels.

(3) The advantage of these Pareto-based approaches is the ability of dealing effectively with more than one objective in a high-dimension search domain. NSGA-II is a fast algorithm with a low level of complexity and the methodology explained in this paper can be used for addressing the calibration of other similar models in the field of hydroinformatics.

(4) Further work is required to find a more reliable method for dividing the cross sections into an appropriate number of efficient panels. Examining other channels, with different cross sections and types of boundary roughness, should give an insight into how to interpret the vast number of calibration results based on the physics of the flow. This will lead to more robust parameter guideline equations, the correct selection of each parameter in each panel, as well as the sign pattern of the secondary flow term, Γ.

REFERENCES

Abril, J. B. & Knight, D. W. 2004 Stage-discharge prediction for rives in flood applying a depth-averaged model. *J. Hydraul. Res.* **42** (6), 616–629.

Al-Hamid, A. A. I. 1991 *Boundary Shear Stress and Velocity Distributions in Differentially Roughened Trapezoidal Open Channels*. PhD Thesis. University of Birmingham, Birmingham.

Anderson, J. D. 1997 *A History of Aerodynamics and Its Impact on Flying Machines*. Cambridge University Press, Cambridge.

Babayan, A. V., Savic, D. A. & Walters, G. A. 2005 Multiobjective optimization for the least-cost design of water distribution systems under correlated uncertain parameters. In *World Water Congress 2005, Impacts of Global Climate Change, World Water and Environmental Resources Congress, Anchorage, AK, 15–19 May* (ed. in R. Walton),.

Bekele, E. G. & Nicklow, J. W. 2007 Multi-objective automatic calibration of SWAT using NSGA-II. *J. Hydrol.* **341**, 165–176.

Bousmar, D. & Zech, Y. 2004 Velocity distribution in non-prismatic compound channels. *Proc. Inst. Civil Eng. Water Manage.* **157**, 99–108.

Chlebek, J. & Knight, D. W. 2006 A new perspective on sidewall correction procedures, based on SKM modeling. In *Proc. Int. Conf. on Fluvial Hydraulics (River Flow 2006), Lisbon, Portugal, September* (ed. in R. M. L. Ferreira, E. C. T. L. Alves, G. A. B. Leal & A. H. Cardoso), Vol. 1, pp. 135–144. Taylor & Francis, London.

Deb, K. & Agarwal, R. B. 1995 Simulated binary crossover for continuous search space. *Complex Syst.* **9**, 115–148.

Downloaded from http://iwaponline.com/jh/article-pdf/11/1/31/386331/31.pdf
by guest

Deb, K., Pratap, A., Agarwal, S. & Meyarivan, T. 2002 A fast and elitist multiobjective genetic algorithm: NSGA-II. *IEEE Trans. Evol. Comput.* **6** (2), 182–197.

Ervine, D. A., Babaeyan-Koopaei, K. & Sellin, H. J. 2000 Two-dimensional solution for straight and meandering overbank flows. *J. Hydraul. Eng.* **126** (9), 653–669.

Farina, M. 2001 *Cost-effective Evolutionary Strategies for Pareto Optimal Front Approximation in Multiobjective Shape Design Optimization of Electromagnetic Devices*. PhD Thesis, Department of Electrical Engineering, University of Pavia, Italy.

Fonseca, C. M. & Fleming, P. J. 1995 *Multiobjective Optimization and Multiple Constraint Handling with Evolutionary Algorithms I: A Unified Formulation*. Research report 564, Department of Automatic Control and Systems Engineering, University of Sheffield, Sheffield.

Ghosh, A. & Dehuri, S. N. 2004 Evolutionary algorithms for multi-criterion optimization: a survey. *Int. J. Comput. Inf. Sci.* **2** (1), 38–57.

Goldberg, D. E. 1989 *Genetic Algorithms in Search, Optimization, and Machine Learning*. Addison-Wesley, Boston.

Hirschen, K. & Schafer, M. 2006 A study on evolutionary multi-objective optimization for flow geometry design. *Comput. Mech.* **37** (2), 131–141.

Khare, V., Yao, X. & Deb, K. 2003 Performance scaling of multi-objective evolutionary algorithms. In *Evolutionary Multi-Criterion Optimization: 2nd International Conference, EMO 2003 Lecture Notes in Computer Science* (Eds. Fonseca, C. M., Fleming, P. J., Zitzler E. & Deb, K.) Vol. 2632, Springer-Verlag, Berlin, pp 376–390.

Knight, D. W. 1992 *SERC Flood Channel Facility Experimental Data–Phase A*, Vol. 1–15. School of Civil Engineering, University of Birmingham. Available at: http://www.flowdata.bham.ac.uk

Knight, D. W. & Abril, J. B. 1996 Refined calibration of a depth-averaged model for turbulent flow in a compound channel. *Proc. ICE J. Water Maritime Energy* **118**, 151–159.

Knight, D. W., Omran, M. & Tang, X. 2007 Modelling depth-averaged velocity and boundary shear in trapezoidal channels with secondary flows. *J. Hydraul. Eng. ASCE* **133** (1), 39–47.

Knight, D. W. & Sellin, R. H. J. 1987 The SERC Flood Channel Facility. *J. Inst. Water Environ. Manage.* **1**, 198–204.

Knight, D. W. & Shiono, K. 1996 River channel and floodplain hydraulics. In *Floodplain Processes* (ed. in M. G. Anderson, D. E. Walling & P. D. Bates), pp. 139–181. John Wiley & Sons, New York, ch 5.

Lahanas, M., Baltas, D. & Zamboglou, N. 2003 A hybrid evolutionary algorithm for multi-objective anatomy-based dose optimization in high-dose-rate brachytherapy. *Phys. Med. Biol.* **48**, 399–415.

Lambert, M. F. & Sellin, R. H. J. 1996 Discharge prediction in straight compound channels using the mixing length concept. *J. Hydraul. Res.* **34** (3), 381–394.

Liu, Y., Zhou, C. & Ye, W. J. 2005 A fast optimization method of using non-dominated sorting genetic algorithm (NSGA-II) and 1-nearest neighbor (1NN) classifier for numerical model calibration. In *IEEE Int. Conf. on Granular Computing*, **Vol. 2**, pp. 544–549.

McGahey, C., Samuels, P. G. & Knight, D. W. 2006 A practical approach to estimating the flow capacity of rivers–application and analysis. In *Proc. Int. Conf. on Fluvial Hydraulics (River Flow 2006), Lisbon, Portugal, September* (ed. in R. M. L. Ferreira, E. C. T. L. Alves, J. G. A. B. Leal & A. H. Cardoso), **Vol. 1**, pp. 303–312. Taylor & Francis, London.

Nazemi, A., Yao, X. & Chan, A. H. 2006 Extracting a set of robust pareto-optimal parameters for hydrologic models using NSGA-II and SCEM. In *Proc. 2006 IEEE Congress on Evolutionary Computation (CEC'06), Vancouver, Canada, 16–21 July*, pp. 6792–6799. IEEE Press, Piscataway, NY.

Nezu, I. & Nakagawa, H. 1993 *Turbulence in Open Channel Flow. IAHR Monograph. A.A*. Balkema, Rotterdam.

Patel, V. C. 1965 Calibration of the Preston tube and limitations on its use in pressure gradients. *J. Fluid Mech.* **23**, 185–208.

Perkins, H. J. 1970 The formation of streamwise vorticity in turbulent flow. *J. Fluid Mech.* **44**, 721–740.

Radojkovic, B. E. & Djordjevic, B. E. 1985 Computation of discharge distribution in compound channels. In: *Proc. 21st IAHR Congr., Melbourne, Australia, 19–23 August*.

Reed, P., Kollat, J. B. & Devireddy, V. K. 2007 Using interactive archives in evolutionary multiobjective optimization: a case study for long-term groundwater monitoring design. *Environ. Model. Softw.* **22**, 683–692.

Samuels, P. G. 1988 Lateral shear layers in compound channels. In: *Proc. Int. Conf. on Fluvial Hydraulics, Budapest*.

Samuels, P. G. 1989 Some analytical aspects of depth averaged flow models. In: *Proc. Int. Conf. on Hydraulic and Environmental Modelling of Coastal, Estuarine and River Waters, Bradford, UK, 19–21 September*.

Schlichting, H. 1979 *Boundary-Layer Theory*, 7th edition. McGraw-Hill, New York.

Shiono, K. & Knight, D. W. 1988 Two-dimensional analytical solution for a compound channel. In *Proc. 3rd Int. Symposium on Refined Flow Modelling and Turbulence Measurements*, pp. 591–599. Universal Academy Press, Tokyo.

Shiono, K. & Knight, D. W. 1990 Mathematical models of flow in two or multi stage straight channels. In *Proc. Int. Conf. on River Flood Hydraulics* (ed. in W. R. White), pp. 229–238. John Wiley & Sons, Chichester, Paper G1.

Shiono, K. & Knight, D. W. 1991 Turbulent open-channel flows with variable depth across the section. *J. Fluid Mech.* **222**, 617–646.

Spooner, J. & Shiono, K. 2003 Modelling of meandering channels for overbank flow. *Proc. ICE J. Water Maritime Energy* **56**, 225–233.

Sun, D., Benekohal, R. F. & Waller, S.T. 2003 *Multi-objective Traffic Signal Timing Optimization Using Non-dominated Sorting Genetic Algorithm II. Lecture Notes in Computer Science*. Vol. 2724, Springer-Verlag, Berlin, pp. 2420–2421. doi: 10.1007/3-540-45110-2_143

Downloaded from http://iwaponline.com/jh/article-pdf/11/1/31/386331/31.pdf
by guest

Tominaga, A., Nezu, I., Ezaki, K. & Nakagawa, H. 1989 Three-dimensional turbulent structure in straight open channel flows. *J. Hydraul. Res.* **7**, 149–173.

Vreugdenhil, C. B. & Wijbenga, J. H. A. 1982 Computation of flow patterns in rivers. *J. Hydraul. Div. ASCE* **108** (11), 1296–1309.

Wormleaton, P. R. 1988 Determination of discharge in compound channels using the dynamic equation for lateral velocity distribution. In: *Proc. Int. Conf. on Fluvial Hydraulics, Budapest, Hungary,* pp. 98–103.

Yuen, K. W. H. 1989 *A Study of Boundary Shear Stress, Flow Resistance and Momentum Transfer in Open Channels with Simple and Compound Trapezoidal Cross Sections*. Ph.D. Thesis, University of Birmingham, Birmingham.

First received 22 April 2008; accepted in revised form 22 September 2008

Downloaded from http://iwaponline.com/jh/article-pdf/11/1/31/386331/31.pdf
by guest